RESEARCH ARTICLE

WILEY

Natural overlaying behaviors push the limit of planar cyclic deformation performance in few-layer MoS$_2$ nanosheets

Peifeng Li[1] | Guangjie Zhang[2] | Zhuo Kang[3,4] | Xin Zheng[5] |
Yong Xie[3,4] | Chunyuan Liang[6] | Yizhi Zhang[6] | Xiaoyang Fang[6] |
Rong Sun[1] | Zhiquan Liu[1] | Yeqiang Bu[6] | Yang Lu[7] | Yue Zhang[3,4]

[1]Shenzhen Institute of Advanced Electronic Materials, Shenzhen Institute of Advanced Technology, Chinese Academy of Sciences, Shenzhen, the People's Republic of China

[2]CAS Key Laboratory of Standardization and Measurement for Nanotechnology, CAS Center for Excellence in Nanoscience, National Center for Nanoscience and Technology, Beijing, the People's Republic of China

[3]Beijing Advanced Innovation Center for Materials Genome Engineering, Beijing Key Laboratory for Advanced Energy Materials and Technologies, University of Science and Technology Beijing, Beijing, the People's Republic of China

[4]State Key Laboratory for Advanced Metals and Materials, School of Materials Science and Engineering, University of Science and Technology Beijing, Beijing, the People's Republic of China

[5]College of Chemistry and Materials Engineering, Zhejiang A&F University, Hangzhou, the People's Republic of China

[6]Center for X-mechanics, School of Aeronautics and Astronautics, Zhejiang University, Hangzhou, People's Republic of China

[7]Department of Mechanical Engineering, The University of Hong Kong, Hong Kong, the People's Republic of China

Correspondence
Peifeng Li, Shenzhen Institute of Advanced Electronic Materials, Shenzhen Institute of Advanced Technology, Chinese Academy of Sciences, Shenzhen 518055, the People's Republic of China.
Email: pf.li1@siat.ac.cn

Yeqiang Bu, Center for X-mechanics, School of Aeronautics and Astronautics, Zhejiang University, Hangzhou 310027, the People's Republic of China.
Email: yeqiangbu@zju.edu.cn

Yang Lu, Department of Mechanical Engineering, The University of Hong Kong, Pokfulam, Hong Kong 999077, the People's Republic of China.
Email: ylu1@hku.hk

Yue Zhang, Beijing Advanced Innovation Center for Materials Genome Engineering, Beijing Key Laboratory for Advanced Energy Materials and Technologies, University of Science and Technology Beijing, Beijing 100083, the

Abstract

As a typical two-dimensional (2D) transition metal dichalcogenides (TMDCs) material with nonzero band gap, MoS$_2$ has a wide range of potential applications as building blocks in the field of nanoelectronics. The stability and reliability of the corresponding nanoelectronic devices depend critically on the mechanical performance and cyclic reliability of 2D MoS$_2$. Although an in situ technique has been used to analyze the mechanical properties of 2D materials, the cyclic mechanical behavior, that is, fatigue, remains a major challenge in the practical application of the devices. This study was aimed at analyzing the planar cyclic performance and deformation behavior of three-layer MoS$_2$ nanosheets (NSs) using an in situ transmission electron microscopy (TEM) variable-amplitude uniaxial low-frequency and cyclic loading–unloading tensile acceleration test. We also elucidated the strengthening effect of the natural overlaying affix fragments (other external NSs) or wrinkle folds (internal folds from the NS itself) on cycling performances and service life of MoS$_2$ NSs by delaying the whole process of fatigue crack initiation, propagation, and fracture. The results have been confirmed by molecular dynamics (MDs) simulations. The overlaying enhancement effect effectively ensures the long-term

Peifeng Li, Guangjie Zhang, Zhuo Kang, and Xin Zheng contributed equally to this work.

People's Republic of China.
Email: yuezhang@ustb.edu.cn

reliability and stability of nanoelectronic devices made of few-layer 2D materials.

KEYWORDS

cyclic deformation performance, few-layer MoS_2, in situ TEM, nanomechanics, natural overlays, strengthening effect

1 | INTRODUCTION

Two-dimensional (2D) transition metal dichalcogenides materials with nonzero band gaps have a wide range of potential applications in the field of nanoelectronics.[1–7] The typical representative, viz., MoS_2, has widespread applications in nano-transistors, memory cells, optical switches, piezoelectric and optoelectronic devices, nano-film displays and touch screens, and nanoelectronic mechanics systems (NEMSs).[2,8–14] The stability and reliability of these devices depend critically on the planar mechanical performance of 2D MoS_2. Thus, the determination of the intrinsic strengths of 2D materials has become a research hotspot. The Young's modulus and intrinsic strength of graphene, as measured by atomic force microscopy (AFM),[15,16] are similar to the ideal values obtained by theoretical simulations.[17,18] The approximate intrinsic strengths of the mono- and few-layer MoS_2 were also obtained.[19–23] However, these studies only provide information on the mechanical properties of the local or point area rather than the whole planar performance. Thus, in situ tensile testing is the most effective and intuitive way to study the planar mechanical properties and behaviors of 2D materials. The planar mechanical properties of single-crystalline monolayer graphene, graphene oxide (GO) NSs, multilayer MoS_2 membranes, and polycrystalline hexagonal boron nitride (h-BN) monolayers were determined by in situ scanning electron microscopy (SEM).[24–27] The results demonstrate that single-crystal graphene has an elastic modulus close to the theoretical value of 1 TPa, with an elastic strain of $\sim6\%$.[24] GO NS shows a high tensile strength, close to that of monolayer GO, which has a strong correlation with its effective volume and thickness.[25] The fracture strengths of multilayer MoS_2 membranes have an obvious thickness effect: the thinner the membranes, the higher the fracture strengths.[26] The experimental results revealed that the elastic limit of h-BN is virtually immune to naturally occurring atomic defects and is gradually reduced by the presence of sub-micrometer voids.[27] The results also showed that the precracked graphene and $MoSe_2$ have much lower fracture stress values than their perfect counterparts.[28,29] Moreover, the single-crystal monolayer h-BN has high fracture toughness owing to crack deflection and branching, with an effective energy release rate that is higher than that of graphene by up to one order of magnitude.[30] In situ transmission electron microscopy (TEM) was also used to elucidate the planar mechanical properties and behaviors of multilayer graphene, GO, MoS_2, hybrid graphene film with Ag nanowires (NWs), and rebar graphene.[31–37] The results revealed that the fracture strength of multilayer graphene decreases with increasing thickness owing to the defects in the fractured layers, and the fracture has obvious delamination between the atomic layers.[32] Multilayer GO has higher fracture toughness than graphene.[33] It was found that the cracks in monolayer MoS_2 propagated with atomically sharp tips in the preferred direction with the least amount of energy release, and the fracture mode shifted from brittle to ductile on increasing the defect density.[34] Dislocation emission in monolayer MoS_2 was closely associated with the crack propagation path as revealed by the analysis of the atomic structures and dislocation dynamics in the crack tip zone.[35] Interestingly, the embedded Ag NWs and carbon nanotubes (CNTs) can effectively enhance the toughness of graphene.[36,37]

Although significant progress has been made by using the in situ technique, it cannot reflect the real planar stress states and mechanical behaviors of 2D materials in practical applications. Owing to their sizes, working

conditions, and external surroundings, 2D materials endure electrical, thermal, and mechanical fatigue, which may pose significant challenges in their applications. The in situ TEM resonance and digital micromirror device (DMD) methods are not suitable for analyzing 2D materials.[38–40] Thus, AFM was used to study the fatigue and fracture strength of graphene, GO, Al_2O_3-graphene nanolayers. The mono- and few-layer graphene exhibited a fatigue life of more than 10^9 cycles at a mean stress of 71 GPa.[41–43] The high elastic strain and fracture stress of single-crystal Si NWs were also obtained by in situ SEM-based uniaxial loading–unloading tensile tests.[44] Based on the above experiences, in this study, we conducted in situ TEM variable-amplitude uniaxial low-frequency and cyclic loading–unloading tensile acceleration tests to study the planar cyclic performance and deformation behavior of few-layer MoS_2 NSs.

Nowadays, the main methods for preparing two-dimensional (2D) materials include mechanical exfoliation, chemical vapor deposition (CVD), liquid exfoliation or synthesis, and so on.[45] Mechanical exfoliation can produce 2D materials with better crystal quality and performance but lower efficiency; while the other two methods have higher efficiency preparation but worse crystal quality and performance. How to simultaneously achieve efficient preparation and high crystal quality or perfect performance is a challenge in current 2D material preparation. We also studied the enhancing effect of natural overlaying behaviors of few-layer MoS_2 on their cyclic performance and service life, to obtain an effective method for ensuring the long-term reliability and stability of 2D materials.

2 | RESULTS AND DISCUSSION

MoS_2 NSs were synthesized via chemical vapor deposition (CVD) (see part 3 of Section 4: E.S. 3). The visible light microscopy (VLM), TEM (inset: the optical image and SAED pattern), and STEM images of the MoS_2 NS (Figure S1a,b; Supporting Information) reveal its large size and uniform polycrystalline structures. Its thickness (t) of 3 nm was determined from the AFM height image of MoS_2 NS (Figure S1c). Thus, the number of atomic layers was determined to be 3 (see details in the caption of Figure S1). The peak position difference between A_{1g} and E_{2g} in the Raman spectrum characterization of the MoS_2 NS is about 24.5 cm^{-1}, which is also consistent with the three-layer MoS_2 in previous report.[46] The waveform reveals its 2 h phase structure.[47]

The thus-prepared MoS_2 NS was first transferred to the push-to-pull (PTP) device (see E.S. 2). Figure 1A shows the VLM image of the PTP device with a stiffness

coefficient (k) of 1500 N m^{-1}. This image also reveals the positional relationship between the PTP device and the tungsten (W) tip used for applying loading–unloading forces (as shown in the green dotted ellipse). The gap in the red dotted ellipse is the functional test part to support the MoS_2 NS and performs the cyclic loading–unloading test which is very different from the situation of the uncontrollable in-plane tension introduced by the focused electron beam heating.[48] The TEM images show the unloading (top) and loading (bottom) states (Figure 1B). The detailed operation procedure is described in E.S. 3. Movie S1 displays the reciprocating motion of the W tip relative to the semicircular part of the PTP device. Figure 1C shows a three-layer MoS_2 NS on the gap of the PTP device, with an initial width (w_0) of ∼2656 nm. The inset shows the selected-area electron diffraction (SAED) pattern of the NS, which reveals its perfect polycrystalline structure. Most previous studies determined that the influence of grain boundaries (GBs) on the mechanical properties of 2D materials depends on the angle of GBs. Large angle GBs basically do not significantly reduce the strength of 2D materials, and can even be ignored, while small angle GBs can significantly reduce the strength of 2D materials.[16,49–52] Specifically for the test in this article, since all the samples are taken from the same base material, the influence of GBs and layer stacking is equivalent, which can be ignored. We did not discuss it in depth in the article. Professor Lou Jun et al. have simulated the uniaxial tensile behavior of polycrystalline graphene and found that the crack has intergranular and transgranular fracture at the same time, with a brittle fracture general trend.[28] The presence of GBs does not significantly affect the crack propagation and brittle fracture modes of 2D materials.[28,29]

2.1 | Cyclic performance and deformation behavior of three-layer MoS_2 NS without overlays

The cyclic performance and deformation behavior of the three-layer MoS_2 NS without overlays was determined by controlling the XNano-M harmonic software (Figure 1C, see test regulations in E.S. 3). Movie S1-1 shows the first cyclic loading–unloading test with amplitude of 5 V ($A = 4/3*U$ nm, see details in E.S. 3) and frequency of 2 Hz, over 100 cycles. The state of MoS_2 NS after the first cyclic loading–unloading test is observed in Figure 2A. No obvious changes (such as plastic deformation, crack initiation, crack propagation, and fracture) were observed in the NS compared with its initial state before the test (Figure 1C). Subsequently, the external bias was gradually increased by 5 V (adjusting the amplitudes) each time
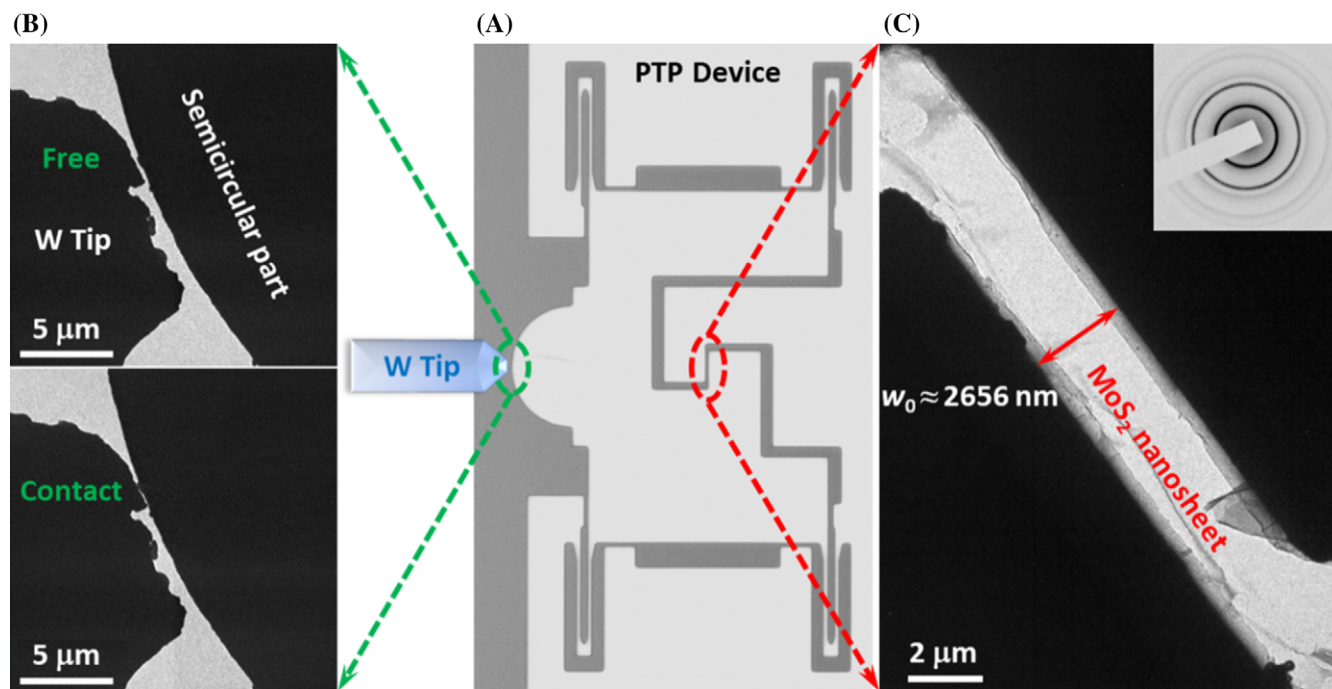
FIGURE 1 Cyclic loading–unloading test equipment and schematic. (A) VLM image of the PTP device. (B) TEM images of the unloading (top) and loading (bottom) states between the W tip and the semicircular part of the PTP device. (C) A three-layer MoS_2 NS on the gap of the PTP device, and its SAED pattern.

the test is repeated. After each cyclic loading–unloading test, the morphologies and characteristics of the NS were observed. The test was repeated till any noticeable change was observed. Movie S1-2 shows the cyclic loading–unloading test with amplitude of 90 V. The state of the MoS_2 NS after conducting the test is observed in Figure 2B. It still showed no obvious changes compared with the initial state (Figure 1C). The cyclic performance and deformation behavior of the MoS_2 NS with amplitudes ranging from 5 V to 90 V are all characteristic of elastic deformation with complete reversibility. Figure S1 and Movie S1-4 show the MD simulations of the cyclic elastic deformation behavior of MoS_2 NS without overlays. The atomic structure of MoS_2 NS in its free state is shown in Figure S1a (the red and blue circles represent the S and Mo atoms, respectively; top: cross section; bottom: the flat). The atomic structure of MoS_2 NS on the PTP device gap before deformation that had been prestressed by gravity is shown in Figure S1b. Figure S1b–f show complete elastic deformation of the MoS_2 NS in one cycle with strains of 0%, 2%, 4%, 2%, and 0%, which can be described by Figure S1d. After the multiple cyclic elastic deformations (Figure S1f), the MoS_2 NS retained its perfect crystalline structure as before (Figure S1b).

As the amplitude increased continuously to 95 V, cracks (defined as fatigue cracks) began to appear in the MoS_2 NS during the cyclic loading–unloading test, as shown in Movie S1-3. The distribution of fatigue cracks

in the MoS_2 NS is observed in Figure 2C. The morphologies and characteristics of the cracks can be observed more clearly in Figure 2D. The cracks can be classified into two types, major (marked with red ellipses) and minor (marked with a yellow ellipses), which were initiated in the functional test gap and the side gaps (perpendicular to the functional gap), respectively. The enlarged morphologies of the two types of cracks are shown in Figure S4. The major cracks were parallel to the edge of the test gap (Figure S4a), almost penetrating the entire gap, while the minor cracks (Figure S4b,c) were inclined at an angle of ∼45° with the edge of the side gaps and the functional test gap (Figure S4b,c). The difference between the two types of cracks reveals the different states of stress of the MoS_2 NS at different sites. The MoS_2 NS on the test gap was in the normal stress state during the cyclic loading–unloading test, while the MoS_2 NS on the side gaps was in the shear stress state. Furthermore, the major cracks (Figure S4a) were not continuous and straight, unlike the brittle fracture of 2D materials in the single uniaxial tensile,[24,26,27] but were divided into three (the green circles) segments, and sometimes even four (the pink circle, two cracks merged) or more. The most likely situation was that the multiple fatigue cracks initiated at the stress concentration zones (similar to the defect sites) during the continuous cyclic loading–unloading process. The tips of the initiated cracks or precracks (invisible at current magnification) induced
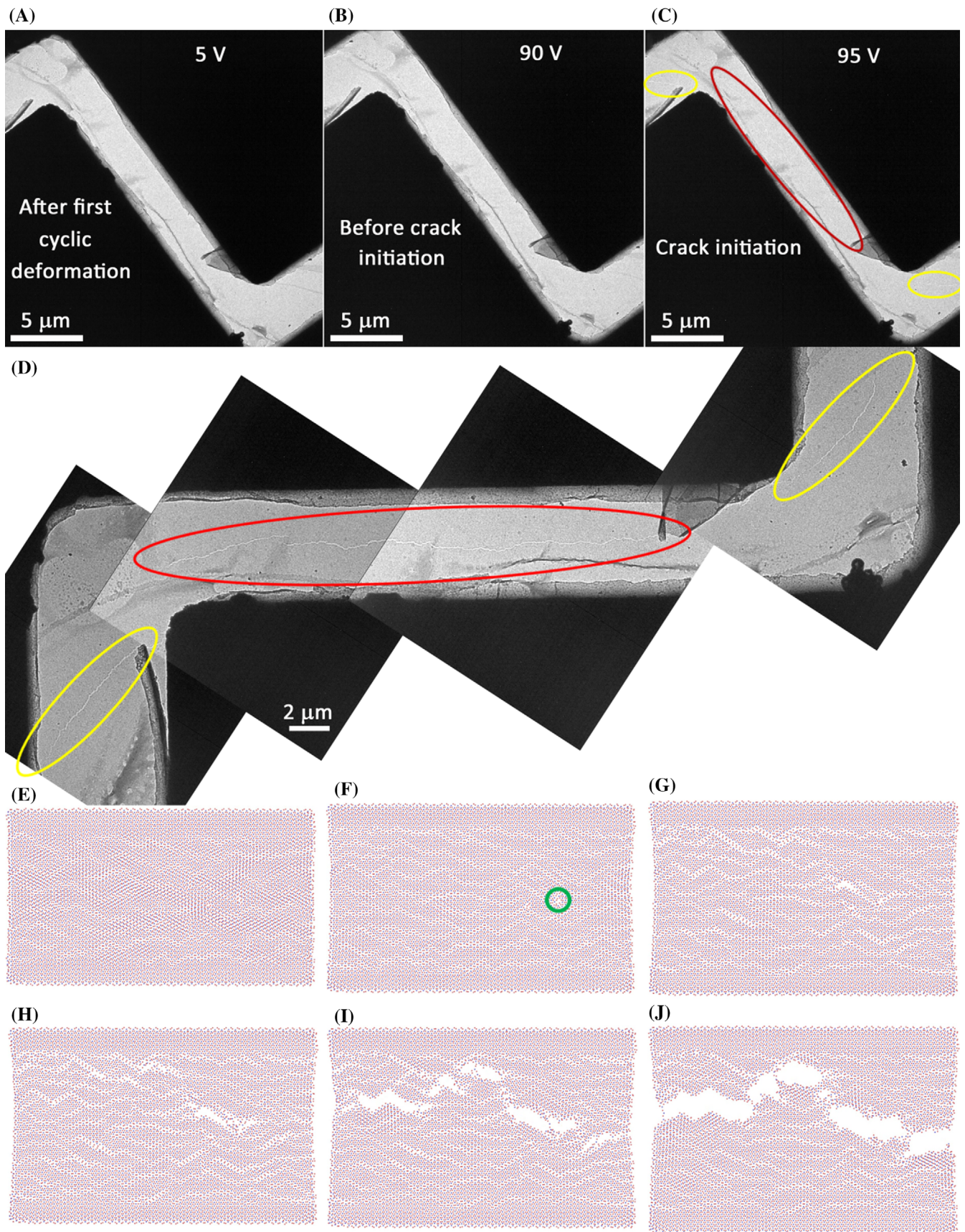
FIGURE 2 Legend on next page.

more pronounced stress concentrations, which led to the crack propagation.[27,28] After continuous propagation, the initial cracks and precracks eventually merged into a few or one major crack. Although the stress states of the MoS$_2$ NS on the side gaps and test gap were different, both types of cracks showed similar shapes and characteristics based on the similar initiation and propagation paths (Figure S4b,c).

The whole cyclic deformation process for MoS$_2$ NS was also verified by MD simulations (Figure 2E–J, Movie S1-5). The atomic structure of MoS$_2$ NS on the PTP test gap before deformation is shown in Figure 2E (The same explanations are omitted in the following text). The NS experienced elastic deformation at the beginning of the cyclic loading–unloading stretching process until a point defect (in the green circle of Figure 2F) was gradually formed that disrupted the original uniform stress distribution. The point defect then gradually expanded into a crack (Figure 2G) with the motion of its surrounding atoms. Furthermore, the initiated crack continued to propagate with the formation of new point defects and cracks (Figure 2H) during the cyclic loading–unloading process. The cracks continued to grow and gradually merged (Figure 2I). Finally, the cracks penetrated the entire NS, making it fractured (Figure 2J). The simulation process is in perfect agreement with the experimentally observed phenomenon.

The experimental cyclic deformation fracture strain (ε) of the MoS$_2$ NS can be calculated by:

$$\varepsilon = \frac{\Delta w}{w_0} = \frac{4/3^* U}{w_0} = \frac{4/3^* 95}{2656} \times 100\% = 4.77\%. \quad (1)$$

Its cyclic deformation fracture strength (σ) can also be estimated by:

$$\sigma = \frac{F}{S} = \frac{\Delta w^* k}{L^* t} = \frac{4/3 \times 95 \times 1500}{19.38 \times 3} = 3.27 \, \text{GPa}. \quad (2)$$

L is the length of the MoS$_2$ NS clamped on the test gap. The cyclic deformation fracture strength of the MoS$_2$ NS is significantly lower than its planar intrinsic or uniaxial tensile strength of 3.97 GPa (Figure S5, the

reduction is as much as 21.41%), which is also consistent with previous reports.[19,22,26,45] Thus, this result indicates that the cyclic performance and deformation behavior (analogy to fatigue) can significantly reduce the fracture strength of 2D materials.
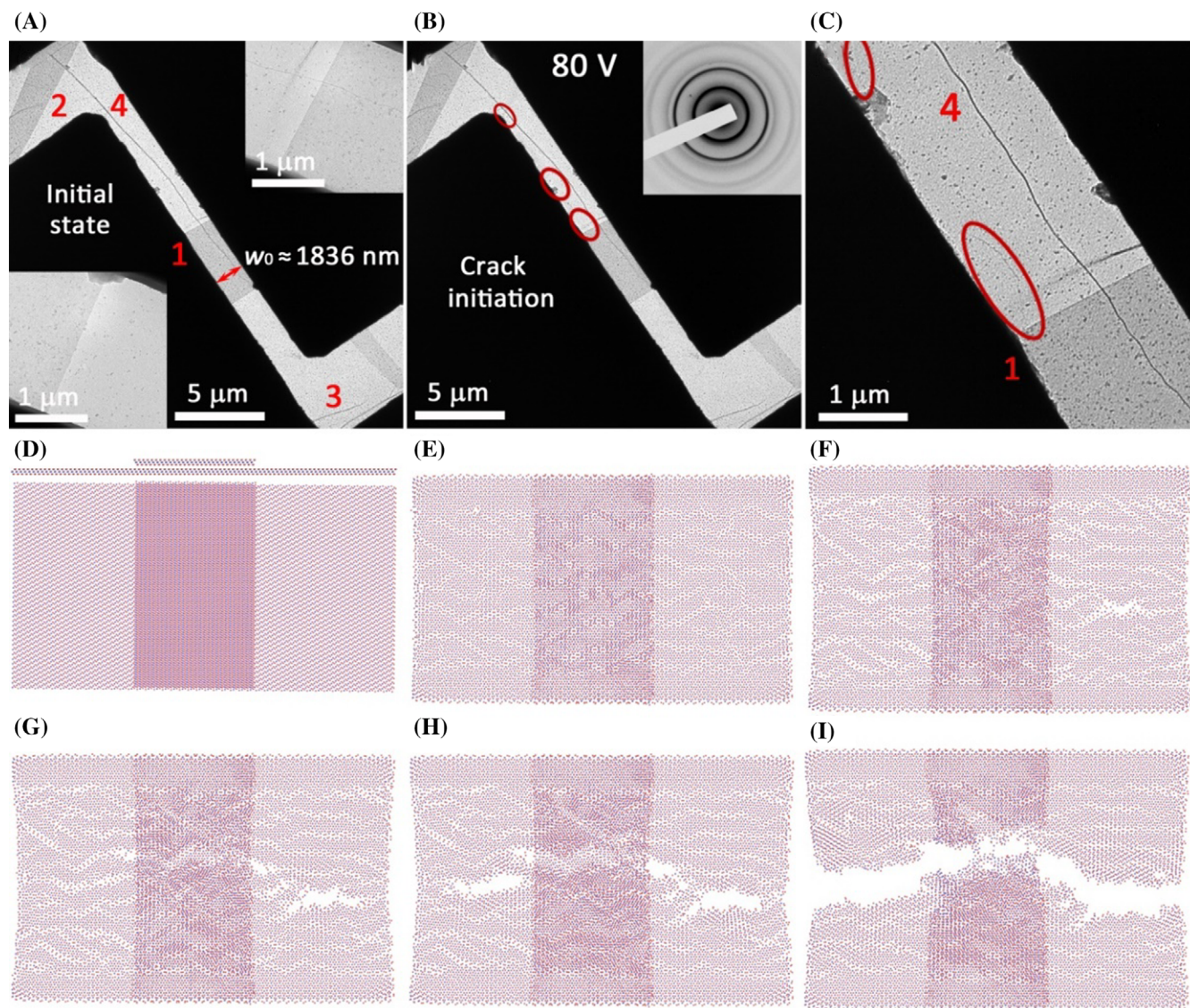
The cyclic performance and deformation behavior of another two MoS$_2$ NSs were measured using the same method. The results are shown in Figure S6. Their cyclic deformation fracture strains were 4.29% and 4.66%, respectively. The average cyclic deformation fracture strain $\bar{\varepsilon}$ of the three MoS$_2$ NSs was $(4.57 \pm 0.25)\%$. Thus, the experimental results are stable and reliable. In accordance with Hooke's law ($\sigma = E\varepsilon$), their average cyclic deformation fracture strength is approximately (3.13 ± 0.17) GPa.

2.2 | Cyclic performance and deformation behavior of three-layer MoS$_2$ NS with affix fragments

In the growth or transfer process, some natural overlaying behavior would occur on the surface of 2D materials, such as affix fragments (other external NSs) or wrinkle folds (internal folds of the NS itself). Figure 3A shows another three-layer MoS$_2$ NS with four overlays marked as 1, 2, 3, and 4. The NS has two types of overlays: affix fragments and wrinkle folds. An affix fragment is formed by stacking another NS on top of the NS (like overlays 1 and 2 in Figure 3A; see the atomic structure in Figure 3D), and a wrinkle fold in NS is formed by stacking its own folds (like overlays 3 and 4 in Figure 3A; see the atomic structure in Figure 4D). The affix fragment 1 (the insets in Figure 3A show its two edges) plays a major role in affecting the cyclic performance and deformation behavior of the NS owing to its location and size.

According to the same test regulation (details in E.S. 3), the cyclic performance and deformation behavior of three-layer MoS$_2$ NS with overlaying of affix fragment was studied. The cyclic elastic deformation tests with amplitude from 5 to 75 V were performed (Movie S3-1). No significant change was witnessed up to this point. However, when the bias was increased to 80 V, fatigue

FIGURE 2 Cyclic performance and deformation behavior of three-layer MoS$_2$ NS without overlays. (A) The state of the MoS$_2$ NS after first cyclic loading–unloading (5 V). (B) The state after multiple cyclic loading–unloading (10, 15, 20, ..., 80, 85, 90 V) before fatigue crack initiation. (C) Fatigue crack initiation and propagation under larger amplitude cyclic loading–unloading (95 V). (D) The enlarged crack in the MoS$_2$ NS (the major cracks in the red ellipse are basically perpendicular to the external force, while the edge cracks in the yellow ellipses are about 45 degrees to the external force). (E) MD simulations of atomic structure of MoS$_2$ NS (the red and blue circles represent the S and Mo atoms, respectively) on the PTP test gap before deformation. (F) A point defect (in the green circle) gradually formed in the cyclic elastic deformation process. (G) Cyclic deformation crack initiated as the movement and expansion of the point defect. (H) The crack continues to propagate and more point defects and crack initiation occur in the cyclic deformation process. (I) The cracks are connected with each other. (J) The cracks penetrates the entire NS which makes the NS fractured.
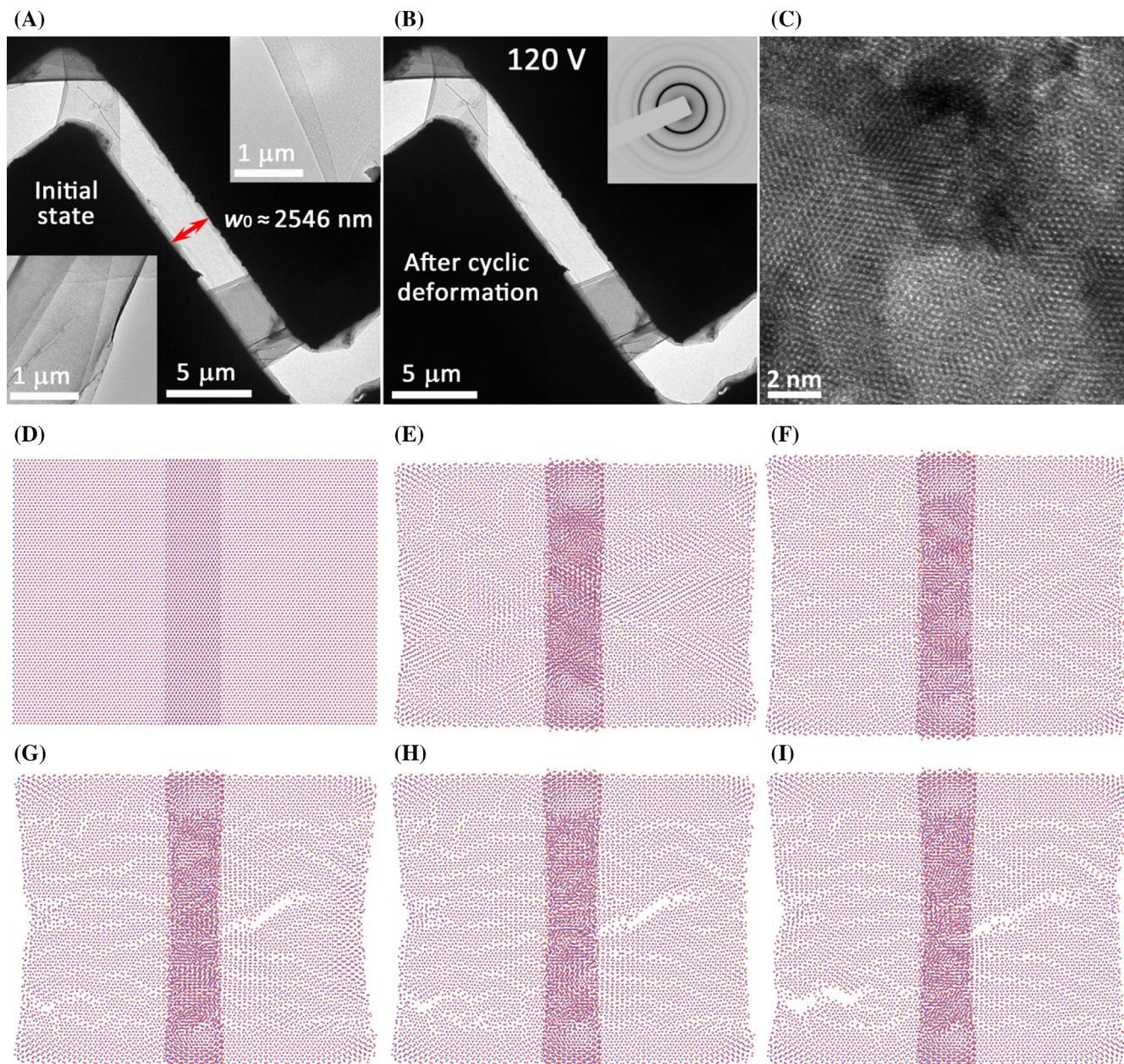
FIGURE 3 Cyclic performance and deformation behavior of three-layer MoS_2 NS with affix fragment. (A) The initial state of the MoS_2 NS marked with four overlays, insets: the two boundaries of the affix fragment 1. (B) The fatigue crack initiation after multiple cyclic loading–unloading (5, 10, ..., 75, 80 V). (C) The enlarged image showing the blocking effect of affix fragment on the crack propagation. (D) MD simulations of atomic structure of the MoS_2 NS with affix fragment under free state (top: cross section; bottom: the flat). (E) Atomic structure of MoS_2 NS with affix fragment on the PTP test gap before deformation. (F) Crack initiation in the elastic cyclic deformation process. (G) The blocking effect of the affix fragment on the propagation of the crack. (H) More crack initiations in the cyclic loading–unloading process. (I) The crack finally penetrates the affix fragment under large cyclic deformation process.

cracks (in red circles) were initiated in the NS, as revealed in Figure 3B. The detailed information can be obtained from Movie S3-2. The morphologies of the initiation of the fatigue cracks are clearly observed (in the red circles) in Figure 3C (enlarged image of Figure 3B). Furthermore, the cracks did not merge together. The experimental cyclic deformation fracture strain of the MoS_2 NS with affix fragment can be calculated by:

$$\varepsilon = \frac{\Delta w}{w_0} = \frac{4/3^*U}{w_0} \times 100\% = \frac{4/3^*80}{1836} \times 100\% = 5.45\%. \quad (3)$$

In accordance with Hooke's law, with the increase in cyclic deformation fracture strain of MoS_2 NS with affix fragment, its fracture strength also increased compared with the one without overlays. Thus, the observation and calculation results reveal that the affix fragment significantly delayed the initiation and propagation of the cracks, and enhanced the cyclic deformation fracture strain and strength of the three-layer MoS_2 NS. This may be because the introduction of the superposition layer is like fastening a safety belt or attaching a piece of tape to the NS, which will change its stress state during cyclic

FIGURE 4 Cyclic performance and deformation behavior of three-layer MoS_2 NS with two-edge wrinkle folds. (A) The initial state of the MoS_2 NS, inset: the enlarged edge images of the overlays. (B) The final state of the MoS_2 NS after cyclic loading–unloading (120 V). (C) STEM of the MoS_2 NS after cyclic loading–unloading which shows perfect crystal and atom arrangement. (D) MD simulations of atomic structure of the MoS_2 NS with wrinkle fold under free state (top: cross section; bottom: the flat). (E) Atomic structure of MoS_2 NS with wrinkle fold on the PTP test gap before deformation. (F) The MoS_2 NS remains elastic deformation during the large strain cyclic deformation test. (G) Fatigue crack initiation during the large strain elastic cyclic deformation test. (H) The blocking effect of the wrinkle fold on the propagation of the crack. (I) The crack eventually stops propagate under the blocking of the wrinkle fold (with larger strain than previous two cases in Figures 2 and 3).

loading–unloading process. The effect is equivalent to reducing the defect concentration in the NS, thus delaying the initiation of cracks. To investigate the effect of the affix fragment (parallel to external forces) on the cyclic performance and deformation behavior of the MoS_2 NS, the propagation of the crack nearby position 1 was observed during the cyclic loading–unloading test with amplitude of 80 V. It was revealed that the crack did not penetrate the affix fragment; however, it continued to propagate forward beneath the overlay at a much slower rate than in the absence of overlays (Movie S3-3). A crack preceding a typical affix fragment, whose propagation rate was greatly decelerated by the blocking of this overlay, can be observed (Figure 6A).

The whole cyclic deformation process of the MoS_2 NS with affix fragment was also verified by MD simulations (Figure 3D–I, Movie S3-5). During the cyclic loading–unloading stretching test, a fatigue crack was initiated in the MoS_2 NS (right-hand-side image in Figure 3F). However, crack propagation was blocked when it encountered the affix fragment (Figure 3G). As the cyclic loading–unloading continued, more fatigue cracks developed, and the previous crack also propagated forward, beneath the affix fragment, at a much lower rate (Figure 3H). Finally, the cracks penetrated the entire NS even in the obstruction of the affix fragment which makes the NS and overlay fractured (Figure 3I). The simulations are also in perfect agreement with previously reported experimental results. Therefore, the affix fragment successfully slows down the initiation and propagation of fatigue cracks in 2D materials, and significantly improves their cyclic performance and deformation behavior.

2.3 | Cyclic performance and deformation behavior of three-layer MoS_2 NS with wrinkle folds

The cyclic performance and deformation behavior of the MoS_2 NS with wrinkle folds (parallel to external forces) was studied. Figure 4A shows another three-layer MoS_2 NS with two-edge wrinkle folds, while the insets show the two edges of the overlays. Movies S4-1 and S4-2 display the first and last cyclic loading–unloading tests with amplitudes of 5 and 120 V, respectively. The final state of the NS after multiple cyclic loading–unloading tests with amplitudes ranging from 5 to 120 V is observed in Figure 4B. No fatigue cracks were initiated in the NS up to this point, indicating the super-strong blocking-effect of wrinkle folds on the crack initiation in 2D materials during the cyclic loading–unloading process. The experimental cyclic deformation strain of the MoS_2 NS with wrinkle folds at 120 V can be calculated as follows:

$$\varepsilon = \frac{\Delta w}{w_0} = \frac{4/3^* U}{w_0} \times 100\% = \frac{4/3^* 120}{2546} \times 100\% = 6.28\%. \quad (4)$$

Compared with the previous two cases, in the absence of fatigue crack initiation, the cyclic deformation strain of the MoS_2 NS with two-edge wrinkle folds reached as high as 6.28%. Furthermore, using Hooke's law, we can infer that the cyclic deformation fracture strength of the MoS_2 NS with wrinkle folds has improved compared to that of the MoS_2 with affix fragments. The two-edge wrinkle folds effectively fix the geometry structure of the MoS_2 NS like the staples, thus significantly delaying the initiation of fatigue cracks, and further improving its

cyclic performance and deformation behavior. Figure 4C and the inset in Figure 4B show the scanning TEM (STEM) image and SAED pattern of the NS, indicating a perfect polycrystalline structure and atom arrangement. Therefore, the multiple cyclic deformations do not impair the crystal structure of the MoS_2 NS.

In fact, the wrinkle fold has a blocking or termination effect on propagation of precracks or initiated fatigue cracks to a certain extent. This can be understood by analyzing the initiated crack nearby the side wrinkle fold 3 in Figure 3A. The propagation of the crack during the cyclic loading–unloading with amplitude of 80 V is shown in Movie S3-4. The propagation of the fatigue crack was terminated once encountering the wrinkle fold (Movie S3-4; Figure 6B).

The whole cyclic deformation process of the MoS_2 NS with wrinkle fold was also verified by MD simulations (Figure 4D–I, Movie S4-3). During the cyclic loading–unloading stretching test, the MoS_2 NS experienced a longer elastic deformation phase (Figure 4F). Then, a fatigue crack was gradually initiated in the NS (Figure 4G). The propagation of the crack was blocked when it encountered the wrinkle fold (Figure 4H). As the cyclic loading–unloading continues, more fatigue cracks were initiated. However, the previous crack failed to penetrate the wrinkle fold, thus terminating its propagation process (Figure 4I). The simulations are also in perfect agreement with the previous experimental phenomenon. The results once again confirm that the wrinkle fold not only delays the initiation of the fatigue cracks in the NS but also blocks or even terminates the propagation of the cracks to a certain extent, which significantly improves the cyclic performance and deformation behavior of 2D materials.

Based on the above experimental results, a graph (Figure 5A) can be plotted to summarize the cyclic performance and deformation behavior of three-layer MoS_2 NS in different states. It is apparent from the graph that natural overlaying of three-layer MoS_2 NS by affix fragments or wrinkle folds can delay the fatigue crack initiation and have a blocking or termination effect on the crack propagation.

2.4 | Acceleration effect of the overlay perpendicular to the direction of external force

It is important to note that not any type of overlay can enhance the cyclic performance and deformation behavior of 2D materials. All the overlays highlighted in previous sections have one common feature: they are all parallel or nearly parallel to the direction of external forces. However, if the orientation of the overlay relative to the direction of external forces changes, so does its
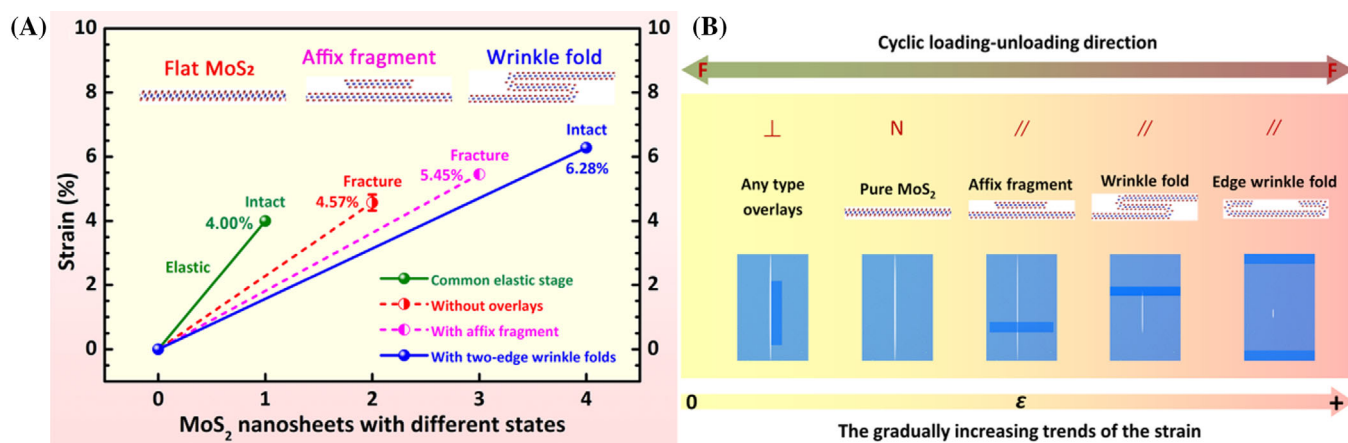
FIGURE 5 (A) The cyclic performance and deformation behavior of three-layer MoS_2 measured in the experimental with different states: without overlays, with affix fragment and two-edge wrinkle folds. (B) Schematic of cyclic deformation performance of three-layer MoS_2 NS with different states as the increasing strain. ⊥, N, and ∥ represent that the direction of the overlays and the external force are vertical, none overlays, and parallel, respectively.
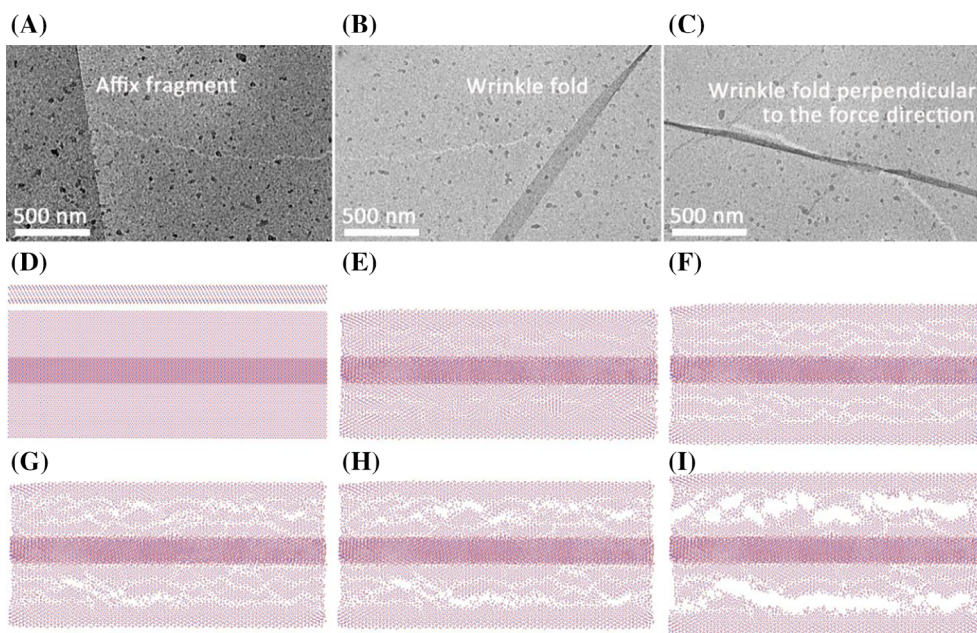
FIGURE 6 Deceleration, termination, and acceleration effect of overlays with different directions to the external force on fatigue crack propagation. (A) Deceleration effect of affix fragment parallel to the external force on crack propagation. (B) Termination effect of wrinkle fold parallel to the external force on crack propagation. (C) Acceleration effect of overlay perpendicular to the external force on crack propagation. (D) MD simulations of the atomic structure of wrinkle fold perpendicular to the external force under free state (top: cross section; bottom: the flat). (E) Atomic structure of MoS_2 NS on the PTP gap before deformation. (F–I) Accelerated fatigue crack initiation and propagation under the cyclic deformation.

effect. We considered the wrinkle fold 4 (perpendicular to the direction of external forces) shown in Figure 3A,C. Once a fatigue crack was initiated in the NS during the cyclic loading–unloading test, it propagated rapidly along the nearby regions of the overlay, where were prone to stress concentrations (Figure 6C). Thus, the overlay perpendicular to the direction of external forces would become the expressway for crack propagation which can

harm the cyclic performance and deformation behavior of 2D materials that should be avoided.

The cyclic deformation process of the MoS_2 NS with wrinkle fold perpendicular to the direction of external forces was simulated by MD method (Figure 6D–I, Movie S4-4). During the cyclic loading–unloading stretching test, the MoS_2 NS experienced a shorter elastic deformation phase and numerous fatigue cracks were

initiated (Figure 6F). The cracks then rapidly propagated (Figure 6G) and merged (Figure 6H), causing the fracturing of NS with overlays (Figure 6I) to be faster than the ones without overlays (Figure 2E–J). Thus, the simulations vividly depict that the overlay perpendicular to the direction of external forces creates an expressway for crack propagation. Therefore, to avoid damaging their cyclic performance and deformation behavior, the distribution of overlays perpendicular to the force direction in 2D materials should be eliminated. In order to be more consistent with the experimental results, we specially simulate the planar cyclic performance and deformation behavior of three-layer 2H phase structure MoS_2 NSs without overlay, with overlay parallel and perpendicular to external force under the same amplitude (that is strain). The results are shown in Figure S3. When the pure three-layer MoS_2 NSs breaks or fails (The arrangement of atoms becomes abnormally loose, which can be judged as failure or fracture of the MoS_2 NS, as marked by the red lines in Figure S3.) normally, the overlay has obvious hindering (//) or accelerating ($\perp$) effect of the fracture according to the direction of the overlay and external force. The MD simulation results also fit well with the results of our experimental results.

The changes of the three-layer MoS_2 NS with different states as the increasing strain was summarized in the schematic image in Figure 5B from which we can quickly and simply distinguish the effects of various natural overlays on the planar cyclic performance and deformation behavior of 2D materials. In short, overlaying of MoS_2 NS by affix fragments or wrinkle folds parallel to the force direction improves its cyclic performance and deformation behavior, and so does its service life. It provides a route that can be imitated (adding foreign overlays) to improve the cyclic deformation fracture strength of 2D materials and corresponding devices for practical applications.

3 | CONCLUSION

In summary, a universal in situ TEM cyclic loading–unloading tensile acceleration test was conducted to study the planar cyclic performance and deformation behavior of 2D materials. The whole process of fatigue crack initiation, propagation, and fracture failure of the three-layer MoS_2 NSs was in situ characterized for the first time, and the MD simulations model was built as an auxiliary method to verify its planar cyclic performance and deformation behavior. With a fracture strain of $(4.57 \pm 0.25)\%$, the experimental cyclic deformation fracture strength of the MoS_2 NS was approximately (3.13 ± 0.17) GPa, which is far lower than its planar intrinsic strength (>3.97 GPa). The natural overlaying affix fragments or wrinkle folds in

the MoS_2 NSs have proved to be effective in enhancing their planar cyclic performance and deformation behavior. The effect of the angle between the natural overlays and external force on the fatigue crack initiation and propagation behavior of the NS is as follows: the effects gradually change from deceleration or termination to acceleration as the angle was increased from $0°$ to $90°$. This study provides a novel idea derived from basic theory and based on practical guidance for the enhancement of planar cyclic mechanical properties of 2D materials and related devices.

4 | EXPERIMENTAL SECTION

4.1 | Materials characterization

The few-layer MoS_2 NS was synthesized by CVD from 6Carcon Technology (Shenzhen, China) Corporation.[6,53] The thickness of the few-layer MoS_2 NS was determined by AFM (Figure S1c), which was found to be 3 nm. The number of the few-layer NSs can be calculated and determined to be 3 (see details in the captions of Figure S1). The peak position difference between A_{1g} and E_{2g} in the Raman spectrum characterization (Figure S1d) of the MoS_2 NS is about $24.5\ cm^{-1}$, which is also consistent with the three-layer MoS_2 in previous report[46]; the waveform reveals its 2 h phase structure.[47] The MoS_2 NS used in the cyclic loading–unloading tests was synthesized in the same manner as few-layer MoS_2 NSs, and share the same number of layers, crystal characteristics or defect concentrations, and mechanical and physical properties under the same conditions.

4.2 | Transfer of few-layer MoS_2 NS

First, the surface of the SiO_2 substrate with CVD-grown three-layer MoS_2 NS was spin-coated with PMMA glue. Furthermore, this coated SiO_2 substrate was immersed in the NaOH solution until the PMMA film (with MoS_2) got detached. Then, the PMMA film was washed several times in the deionized water. Subsequently, the PMMA film was extracted by the PTP device from the deionized water. Finally, the PMMA film was removed using acetone and left to dry, leaving only the three-layer MoS_2 NS on the PTP device.

4.3 | In situ TEM measurement of cyclic performance and deformation behavior of MoS_2 NS

The PTP device with three-layer MoS_2 NS was fixed at one end of the XNano-M TEM holder designed by the

Center for X-Mechanics, Zhejiang University, China. A W tip was fixed on the other end. Then, the XNano-M holder was inserted into the JEM-2100 (JEOL, Japan). The W tip could move freely in three-dimensional space controlled by piezoelectric ceramics. First, the tip was controlled to move forward to the PTP device gradually. Once the tip touched the semicircular part of the PTP device, the PTP device started to be compressed, and the three-layer MoS_2 NS on the gap would be stretched. Then, the cyclic performance and deformation behavior of the three-layer MoS_2 NS was observed by in situ TEM. The cyclic loading–unloading (Figure S1f) parameters, including amplitudes, periodic time (or frequencies), and cyclic number, were adjusted by the XNano-M harmonic software program (Figure S1e). The amplitude was controlled by external bias and was linear to the bias value (*Note*: the amplitude in the article is directly expressed by the bias value). It was set from 5 to 120 V (increasing 5 V each time for the following tests, and the highest bias is 120 V) until obvious changes (fatigue crack initiation, propagation, and fracture) occurred in the three-layer MoS_2 NS. The distance between the W tip and the semicircular of the PTP device was reduced to approximately 160 nm (the yellow segment in Figure S1h) before moving (Figure S1g) and after moving under 120 V (Figure S1h). Thus, the cyclic deformation displacement (or amplitude) of 1 V is about $4/3$ nm ($A = 4/3^*U$ nm). The strain of the MoS_2 NS in the test is given by $\varepsilon = \frac{\Delta w}{w_0} = \frac{4/3^*U}{w_0} \times 100\%$. The larger amplitude is used to compensate for the shortcomings of the low cyclic number. The cyclic number and frequency in the test were set at 100 and 2 Hz, respectively, considering the time of the test (or video capacity) and capture clarity. Thus, considering the frequency, cyclic number, and amplitude, the above test is defined as an in situ TEM variable-amplitude uniaxial low-frequency and cyclic loading–unloading tensile acceleration test.

4.4 | Introduction of MD simulations

The MD simulations software used in the manuscript was the stable version of LAMMPS released on October 19, 2020, which simulated the model construction and data file generation of LAMMPS using Atomsk combined with Avogadro. The initial configuration of MoS_2 is the CIF file with 1T structure, and the ReaxFF potential function force field parameter with better stability is selected to describe the thin MoS_2 film structure.[54] The MD sample sizes chosen in Figure S1/Figures 2, 3, 4, and 6 are $142 \times 250 \times 6.0$ Å^3, $142 \times 250 \times 15.0$ Å^3, $142 \times 250 \times 24.0$ Å^3, and $100 \times 250 \times 24.0$ Å^3, respectively. The four models were constructed respectively under periodic boundary conditions and 300 K, and the

Berendsen temperature control method was used to control the system temperature at 300 ± 10 K. The NVE ensemble was used, and the time step was 0.25 to carry out relaxation for a long enough time (6000 steps). To ensure the reliability of the results, contractile boundary conditions in the X and Y directions and fixed boundary conditions in the Z direction are used in the simulation process. The unit is REAL, the atom type is CHARGE, and the radius of the neighborhood table is 2 bin. The temperature is kept at 300 K and the Berendsen temperature control method is used to control the temperature of the system at 300 ± 10 K, which is the same as the relaxation process. Using the NVE ensemble, the atoms at the upper and lower ends of the system are fixed and loaded with opposite stretching velocities of $\pm 5E^{-4}$ Åps. After 10 000 steps of stretching, reverse the direction of stretching to unload, thus completing a loading–unloading cycle. After ~20 cyclic loading–unloading, the results were imported into the OVITO software for postprocessing.

CONFLICT OF INTEREST STATEMENT
The authors declare no conflict of interest.

ORCID
Peifeng Li https://orcid.org/0000-0002-6722-862X
Yue Zhang https://orcid.org/0000-0002-8213-1420

REFERENCES
1. Mak KF, Lee C, Hone J, Shan J, Heinz TF. Atomically thin MoS_2: a new direct-gap semiconductor. *Phys Rev Lett*. 2010;105(13):105.
2. Radisavljevic B, Radenovic A, Brivio J, Giacometti V, Kis A. Single-layer MoS_2 transistors. *Nat Nanotechnol*. 2011;6(3): 147-150.
3. Voiry D, Yamaguchi H, Li JW, et al. Enhanced catalytic activity in strained chemically exfoliated WS_2 nanosheets for hydrogen evolution. *Nat Mater*. 2013;12(9):850-855.
4. Jones AM, Yu HY, Ghimire NJ, et al. Optical generation of excitonic valley coherence in monolayer WSe_2. *Nat Nanotechnol*. 2013;8(9):634-638.

5. Hong XP, Kim J, Shi SF, et al. Ultrafast charge transfer in atomically thin MoS_2/WS_2 heterostructures. *Nat Nanotechnol.* 2014;9(9):682-686.

6. Zhang XK, Liao QL, Liu S, et al. Poly(4-styrenesulfonate)-induced sulfur vacancy self-healing strategy for monolayer MoS_2 homojunction photodiode. *Nat Commun.* 2017;8(1): 15881.

7. Yoo D, Kim M, Jeong S, Han J, Cheon J. Chemical synthetic strategy for single-layer transition-metal chalcogenides. *J Am Chem Soc.* 2014;136(42):14670-14673.

8. Roy K, Padmanabhan M, Goswami S, et al. Graphene–MoS_2 hybrid structures for multifunctional photoresponsive memory devices. *Nat Nanotechnol.* 2013;8(11):826-830.

9. Yu WJ, Liu Y, Zhou HL, et al. Highly efficient gate-tunable photocurrent generation in vertical heterostructures of layered materials. *Nat Nanotechnol.* 2013;8(12):952-958.

10. Lien DH, Amani M, Desai SB, et al. Large-area and bright pulsed electroluminescence in monolayer semiconductors. *Nat Commun.* 2018;9(1):9.

11. Choi M, Park YJ, Sharma BK, Bae SR, Kim SY, Ahn JH. Flexible active-matrix organic light-emitting diode display enabled by MoS_2 thin-film transistor. *Sci Adv.* 2018;4(4):4.

12. Wu WZ, Wang L, Li YL, et al. Piezoelectricity of single-atomic-layer MoS_2 for energy conversion and piezotronics. *Nature.* 2014;514(7523):470-474.

13. Qi JJ, Lan YW, Stieg AZ, et al. Piezoelectric effect in chemical vapour deposition-grown atomic-monolayer triangular molybdenum disulfide piezotronics. *Nat Commun.* 2015;6:7430.

14. Lee J, Wang ZH, He KL, Yang R, Shan J, Feng PXL. Electrically tunable single- and few-layer MoS_2 nanoelectromechanical systems with broad dynamic range. *Sci Adv.* 2018; 4(3):4.

15. Lee C, Wei XD, Kysar JW, Hone J. Measurement of the elastic properties and intrinsic strength of monolayer graphene. *Science.* 2008;321(5887):385-388.

16. Lee GH, Cooper RC, An SJ, et al. High-strength chemical-vapor–deposited graphene and grain boundaries. *Science.* 2013; 340(6136):1073-1076.

17. Khare R, Mielke SL, Paci JT, et al. Coupled quantum mechanical/molecular mechanical modeling of the fracture of defective carbon nanotubes and graphene sheets. *Phys Rev B.* 2007;75(7):75.

18. Liu F, Ming PM, Li J. Ab initio calculation of ideal strength and phonon instability of graphene under tension. *Phys Rev B.* 2007;76(6):76.

19. Bertolazzi S, Brivio J, Kis A. Stretching and breaking of ultrathin MoS_2. *ACS Nano.* 2011;5(12):9703-9709.

20. Castellanos-Gomez A, Poot M, Steele GA, van der Zant HSJ, Agrait N, Rubio-Bollinger G. Elastic properties of freely suspended MoS_2 nanosheets. *Adv Mater.* 2012;24(6):772-775.

21. Liu K, Yan QM, Chen M, et al. Elastic properties of chemical-vapor-deposited monolayer MoS_2, WS_2, and their bilayer heterostructures. *Nano Lett.* 2014;14(9):5097-5103.

22. Lorenz T, Joswig JO, Seifert G. Stretching and breaking of monolayer MoS_2—an atomistic simulation. *2D Mater.* 2014;1(1): 011007.

23. Joswig JO, Lorenz T, Wendumu TB, Gemming S, Seifert G. Optics, mechanics, and energetics of two-dimensional MoS_2 nanostructures from a theoretical perspective. *Acc Chem Res.* 2015;48(1):48-55.

24. Cao K, Feng SZ, Han Y, et al. Elastic straining of free-standing monolayer graphene. *Nat Commun.* 2020;11(1):11.

25. Cao CH, Daly M, Chen B, et al. Strengthening in graphene oxide nanosheets: bridging the gap between interplanar and intraplanar fracture. *Nano Lett.* 2015;15(10):6528-6534.

26. Li PF, Jiang CC, Xu S, et al. In situ nanomechanical characterization of multi-layer MoS_2 membranes: from intraplanar to interplanar fracture. *Nanoscale.* 2017;9(26):9119-9128.

27. Han Y, Feng SZ, Cao K, et al. Large elastic deformation and defect tolerance of hexagonal boron nitride monolayers. *Cell Rep Phys Sci.* 2020;1(8):1.

28. Zhang P, Ma LL, Fan FF, et al. Fracture toughness of graphene. *Nat Commun.* 2014;5(1):5.

29. Yang YC, Li X, Wen MR, et al. Brittle fracture of 2D $MoSe_2$. *Adv Mater.* 2017;29(2):29.

30. Yang YC, Song ZG, Lu GY, et al. Intrinsic toughening and stable crack propagation in hexagonal boron nitride. *Nature.* 2021; 594(7861):57-61.

31. Wei XL, Xiao S, Li FX, et al. Comparative fracture toughness of multilayer graphenes and boronitrenes. *Nano Lett.* 2015;15(1): 689-694.

32. Li PF, Cao K, Jiang CC, et al. In situ tensile fracturing of multilayer graphene nanosheets for their in-plane mechanical properties. *Nanotechnology.* 2019;30: 475708.

33. Cao CH, Mukherjee S, Howe JY, et al. Nonlinear fracture toughness measurement and crack propagation resistance of functionalized graphene multilayers. *Sci Adv.* 2018;4(4):4.

34. Wang SS, Qin Z, Jung GS, et al. Atomically sharp crack tips in monolayer MoS_2 and their enhanced toughness by vacancy defects. *ACS Nano.* 2016;10(11):9831-9839.

35. Ly TH, Zhao J, Cichocka MO, Li LJ, Lee YH. Dynamical observations on the crack tip zone and stress corrosion of two-dimensional MoS_2. *Nat Commun.* 2017;8:14116.

36. Cao K, Yang HK, Gao LB, et al. In situ mechanical characterization of silver nanowire/graphene hybrids films for flexible electronics. *Int J Smart Nano Mat.* 2020;11(3):265-276.

37. Hacopian EF, Yang YC, Ni B, et al. Toughening graphene by integrating carbon nanotubes. *ACS Nano.* 2018;12(8):7901-7910.

38. Gao ZY, Ding Y, Lin SS, Hao Y, Wang ZL. Dynamic fatigue studies of ZnO nanowires by in-situ transmission electron microscopy. *Phys Status Solidi-R.* 2009;3(7-8):260-262.

39. Li PF, Liao QL, Yang SZ, et al. In situ transmission electron microscopy investigation on fatigue behavior of single ZnO wires under high-cycle strain. *Nano Lett.* 2014;14(2):480-485.

40. Jiang CC, Hu DY, Lu Y. Digital micromirror device (DMD)-based high-cycle torsional fatigue testing micromachine for 1D nanomaterials. *Micromachines.* 2016;7(3):7.

41. Cui T, Mukherjee S, Sudeep PM, et al. Fatigue of graphene. *Nat Mater.* 2020;19(4):405-411.

42. Najafi F, Wang GR, Cui T, et al. Fatigue resistance of atomically thin graphene oxide. *Carbon.* 2021;183:780-788.

43. Amirmaleki M, Cui T, Zhao Y, et al. Fracture and fatigue of Al_2O_3-graphene nanolayers. *Nano Lett.* 2021;21(1):437-444.

44. Zhang HT, Tersoff J, Xu S, et al. Approaching the ideal elastic strain limit in silicon nanowires. *Sci Adv.* 2016;2(8):2.

45. Li PF, Kang Z, Zhang Z, et al. In situ microscopy techniques for characterizing the mechanical properties and deformation behavior of two-dimensional (2D) materials. *Mater Today.* 2021;51:247-272.

46. Zheng J, Yan X, Lu Z, et al. High-mobility multilayered MoS$_2$ flakes with low contact resistance grown by chemical vapor deposition. *Adv Mater.* 2017;29(13):1604540.

47. Yu Y, Nam GH, He Q, et al. High phase-purity 1T′-MoS$_2$- and 1T′-MoSe$_2$-layered crystals. *Nat Chem.* 2018;10(6):638-643.

48. Jung GS, Wang S, Qin Z, Martin-Martinez FJ, Warner JH, Buehler MJ. Interlocking friction governs the mechanical fracture of bilayer MoS$_2$. *ACS Nano.* 2018;12(4):3600-3608.

49. Grantab R, Shenoy VB, Ruoff RS. Anomalous strength characteristics of tilt grain boundaries in graphene. *Science.* 2010; 330(6006):946-948.

50. Wei Y, Wu J, Yin H, Shi X, Yang R, Dresselhaus M. The nature of strength enhancement and weakening by pentagon–heptagon defects in graphene. *Nat Mater.* 2012; 11(9):759-763.

51. Rasool HI, Ophus C, Klug WS, Zettl A, Gimzewski JK. Measurement of the intrinsic strength of crystalline and polycrystalline graphene. *Nat Commun.* 2013;4(1):2811.

52. Zhang H, Yu Y, Dai X, et al. Probing atomic-scale fracture of grain boundaries in low-symmetry 2D materials. *Small.* 2021; 17(51):2102739.

53. Lin P, Zhu LP, Li D, Xu L, Pan CF, Wang ZL. Piezo-phototronic effect for enhanced flexible MoS$_2$/WSe$_2$ van der Waals photodiodes. *Adv Funct Mater.* 2018;28(35):28.

54. Ostadhossein A, Rahnamoun A, Wang YX, et al. ReaxFF reactive force-field study of molybdenum disulfide (MoS$_2$). *J Phys Chem Lett.* 2017;8(3):631-640.

SUPPORTING INFORMATION

Additional supporting information can be found online in the Supporting Information section at the end of this article.